Biomechanics and Modeling in Mechanobiology (2020) 19:1765–1780
https://doi.org/10.1007/s10237-020-01307-6

ORIGINAL PAPER

Study of the combined effects of PTH treatment and mechanical loading in postmenopausal osteoporosis using a new mechanistic PK-PD model

Maxence Lavaill[1] · Silvia Trichilo[2] · Stefan Scheiner[3] · Mark R. Forwood[4] · David M. L. Cooper[5] · Peter Pivonka[1]

Received: 10 December 2019 / Accepted: 7 February 2020 / Published online: 25 February 2020

Abstract
One of only a few approved and available anabolic treatments for severe osteoporosis is daily injections of PTH (1-34). This drug has a specific dual action which can act either anabolically or catabolically depending on the type of administration, i.e. intermittent or continuous, respectively. In this paper, we present a mechanistic pharmacokinetic–pharmacodynamic model of the action of PTH in postmenopausal osteoporosis. This model accounts for anabolic and catabolic activities in bone remodelling under intermittent and continuous administration of PTH. The model predicts evolution of common bone biomarkers and bone volume fraction (*BV/TV*) over time. We compared the relative changes in *BV/TV* resulting from a daily injection of 20 µg of PTH with experimental data from the literature. Simulation results indicate a site-specific bone gain of 8.66% (9.4 ± 1.13%) at the lumbar spine and 3.14% (2.82 ± 0.72%) at the femoral neck. Bone gain depends nonlinearly on the administered dose, being, respectively, 0.68%, 3.4% and 6.16% for a 10, 20 and 40 µg PTH dose at the FN over 2 years. Simulations were performed also taking into account a bone mechanical disuse to reproduce elderly frail subjects. The results show that mechanical disuse ablates the effects of PTH and leads to a 1.08% reduction of bone gain at the FN over a 2-year treatment period for the 20 µg of PTH. The developed model can simulate a range of pathological conditions and treatments in bones including different PTH doses, different mechanical loading environments and combinations. Consequently, the model can be used for testing and generating hypotheses related to synergistic action between PTH treatment and physical activity.

Keywords Postmenopausal osteoporosis · Dual action of PTH · Bone remodelling model · Pharmacokinetics pharmacodynamics · Mechanical feedback · Site-specific bone response

1 Introduction

Bone remodelling is the lifelong process of bone resorption and bone formation maintaining bone health (Langdahl et al. 2016). In osteoporosis, bone resorption prevails over bone formation and leads to low bone mineral density (BMD) and loss of structural integrity of bone tissue. This causes increased bone fragility and, ultimately, bone fractures (Ferrari 2014). The aim of drug development for osteoporosis (OP) in clinical pharmacology is to decrease the risk of fractures by manipulating the bone remodelling process and by blocking or even counteracting the pathophysiological mechanisms. Available drug treatments are distinguished into anti-catabolic and anabolic drugs (Riggs and Parfitt 2005). The former act to reduce osteoclastic resorption, whereas the latter boost osteoblastic activity, inducing bone formation.

In 2002, teriparatide (Forteo), the 1-34 amino terminal fragment of PTH, was the first anabolic agent to be approved

✉ Maxence Lavaill
maxence.lavaill@qut.edu.au

1 Biomechanics and Spine Research Group, Queensland University of Technology, Brisbane, QLD, Australia

2 St Vincent's Department of Surgery, University of Melbourne, Melbourne, VIC, Australia

3 Institute for Mechanics of Materials and Structures, Vienna University of Technology (TU Wien), Vienna, Austria

4 School of Medical Science, Griffith University, Gold Coast, QLD, Australia

5 Department of Anatomy, Physiology and Pharmacology, University of Saskatchewan, Saskatoon, Canada

by the FDA for the treatment of OP (Saag et al. 2007). Since then, several PTH and PTH-related peptide (PTHrP) derivatives have been developed for treatment of OP (Canalis 2018). Teriparatide is used as a treatment for postmenopausal women and men at high risk for osteoporotic fracture, as identified from a very low T-score obtained from dual-energy X-ray absorptiometry (DEXA) (Saag et al. 2007). The effects of teriparatide on the treatment of osteoporosis have been studied in postmenopausal women and in men, as well as in subjects with glucocorticoid-induced osteoporosis (Saag et al. 2007; Neer et al. 2001). Teriparatide subcutaneously administered at a daily dose of 20 µg increases vertebral and femoral BMD over a 21-month period and causes a 65% reduction in the incidence of vertebral fractures and a 54% reduction in non-vertebral fractures (Neer et al. 2001). Based on safety measures, the long-term exposure to teriparatide is limited to 2 years as the drug can potentially increase the risk of developing osteosarcomas (Subbiah et al. 2010).

The objective of this paper is to develop a mechanistic pharmacokinetic pharmacodynamic (PK/PD) model of the action of PTH (1-34) in postmenopausal osteoporosis (PMO) including mechanical feedback. Despite strong evidence of efficacy and safety of PTH, treatment success is affected by a number of factors including the type of drug administration and dose, gender, and severity of bone disease, among others (Dobnig 2004). More recently, also a link between physical activity (i.e. mechanical loading/unloading of bone) and PTH efficacy has been made (Kostenuik et al. 1999; Tanaka et al. 2004; Brent et al. 2018). The aim of the current paper is to include a number of these factors into a comprehensive PK/PD model to predict changes in bone turnover markers and BMD. Utilizing this type of approach allows development of patient-specific PTH treatment regimens based on the subject's disease progression and physiological activity. In this study, data from literature were used to calibrate and validate the computational model. Also, parametric sensitivity analyses were performed to provide insights into the leading mechanisms driving the anabolic action of PTH.

The anabolic action of PTH is due to its direct effects on cells of the osteoblast lineage, including osteoblast precursor cells, active osteoblasts, osteocytes and lining cells. For a comprehensive review of action of PTH on osteoblastic cells, we refer you to Silva and Bilezikian (Silva and Bilezikian 2015). One of the earliest mechanisms on active osteoblasts was reported by Belido et al. indicating that intermittent PTH reduces osteoblast apoptosis (Bellido et al. 2003). The anti-apoptotic actions of PTH include phosphorylation and inactivation of the pro-apoptotic protein BAD, increased expression of survival genes like Bcl-2, increased expression of Runx2, downregulation of the apoptosis inducer CARP-1 (Cell Cycle and Apoptosis Regulatory Protein) and increase in DNA repair. Through these mechanisms, PTH can enhance osteoblastogenesis and increase the osteoblast cell pool.

As reviewed in detail in Trichilo et al. (2019), several mathematical models have been developed to describe the dual action of PTH on bone cells. Most relevant to the current work are the models by Peterson and Riggs (2010) and Trichilo et al. (2019). In these models, the dual action of PTH is achieved via 3 intracellular regulatory molecules responding to the intermitted PTH administration with different dynamics. In the paper by Peterson and Riggs which simulated the treatment of osteoporosis in humans, PTH was assumed to act exclusively on osteoblast apoptosis (Peterson and Riggs 2010). On the other hand, Trichilo et al. simulated PTH administration to a rat model of osteoporosis and assumed that PTH affects both osteoblast apoptosis (via CREB and Runx2) and osteoclast proliferation (via Wnt signalling). Also, the latter model includes activation of bone lining cells due to PTH treatment leading to bone modelling events (Trichilo et al. 2019).

However, none of these papers included mechanical feedback as part of the remodelling process. The latter is particularly important for long treatment regimes and may play an important role for the observed plateau in BMD after 12–24 months of PTH treatment. Furthermore, mechanical feedback might be involved in the rapid bone loss occurring after PTH is discontinued. Hence, the current work extends the aforementioned models with respect to mechanical feedback. The latter will be implemented using the same framework as previously described (Scheiner et al. 2013; Pivonka et al. 2013), i.e. using the strain energy density in the bone matrix which is sensed by osteocytes as a mechanical feedback regulatory quantity. Based on the above discussions, we included the following novel features in the model:

- PTH pharmacokinetics model applied to PMO.
- Dual action of PTH is accounted for via intracellular regulation of the apoptosis rate of active osteoblasts.
- Model calibration and validation based on experimental data from Harris and Dawson-Hugues (1992), Neer et al. (2001) and Leder et al. (2014).

2 Methods

The mechanistic PK-PD model of bone remodelling developed in this paper is based on previous bone cell population models (BCPM) developed by Pivonka and co-workers (Trichilo et al. 2019; Scheiner et al. 2013; Pivonka et al. 2008, 2010, 2013; Pastrama et al. 2018; Martin et al. 2019; Martínez-Reina and Pivonka 2019). In the following sections are described the two major model features consisting of a PK model of PTH in humans and a mechanistic PD model of bone remodelling which is able to reproduce

catabolic and anabolic actions in response to different PTH administration patterns. The investigated administration patterns are continuous and intermittent PTH administration which have catabolic and anabolic effects on bone, respectively. As in previous work (Trichilo et al. 2019), PMO is simulated by increasing the RANKL production rate which leads to increased bone resorption and consequently bone loss. Furthermore, mechanical feedback is incorporated into the model formulation using the strain energy density in the bone matrix as regulatory quantity. The latter feedback regulates osteoblast precursor proliferation in an anabolic fashion, while catabolic feedback is implemented via upregulation of RANKL production. First, we investigate the effects of different doses of PTH treatment on changes in *BV/TV* at different bone sites, i.e. the femoral neck (FN) and the lumbar spine (LS). Second, we investigate whether the effect of PTH treatment is attenuated for less mobile elderly patients, superimposing mechanical disuse to the PTH treatment. Finally, we look at how treatments with anti-catabolic agents might affect anabolic bone response.

2.1 Pharmacokinetics model of PTH (1-34) in human

The developed PK model for PTH is based on the work of Trichilo et al. (2019). It is a one-compartment model which is formulated with respect to the total body blood volume. Consequently, the computed drug concentration refers to the serum concentration. This one-compartment PK model is shown in Fig. 1 and is fully characterized by the two following constants: the absorption rate constant k_a which represents the drug absorption process from the subcutaneous site of injection into the central compartment (i.e. blood/serum), and the elimination rate constant k_e which represents the drug elimination process from the central compartment. The two constants are calculated as follows (Jambekhar and Breen 2012):

$$k_e = \frac{0.693}{t_{1/2}} \tag{1}$$

$$t_{C_{\max}} = \frac{\ln(k_a/k_e)}{k_a - k_e} \tag{2}$$

where $t_{1/2}$ is the half-life of PTH (1-34) and $t_{C_{max}}$ is the time after which PTH (1-34) reaches a maximum serum concentration. Typical values for the PK model of PTH (1-34) are summarized in Table 1 together with references.

We calibrated the PK model based on a single dose of 20 µg of PTH (1-34), which is the regular dose used to treat PMO (Leder et al. 2009). We use the following system of ordinary differential equations (ODEs):

$$\frac{dD}{dt} = -k_a \cdot D \cdot F \tag{3}$$

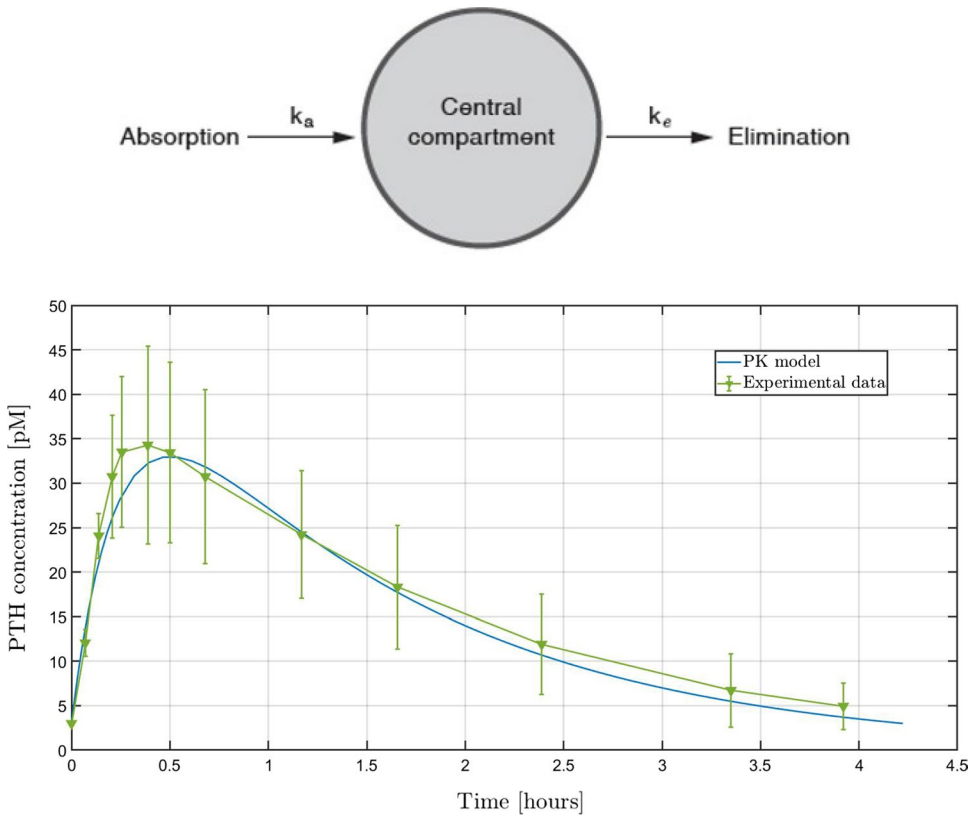

Fig. 1 Top : One-compartment PK model of PTH (1-34): Schematic representation of the model showing the central compartment, the absorption and the elimination process. Bottom : Serum PTH concentration versus time. Blue line shows the PK model simulation. Green line and bars represent experimental data from a 20 µg single injection of teriparatide in a PMO population according to Satterwhite et al. (2010)

Table 1 Pharmacological parameters of subcutaneous PTH (1-34) injection in human PMO population used for the one-compartment PK model of PTH

Parameter	Description	Value	References
$t_{1/2}$	Half-life	1 h	[1,2,3]
$t_{C_{max}}$	Time to max concentration	0.5 h	[1,2,3]
k_e	Elimination rate	0.693 h^{-1}	Computed
k_a	Absorption rate	4.38 h^{-1}	Computed
F	Bioavailability	95%	[1]
V_d	Distribution volume	110 L	[1,3]

Index 1 refers to Eli Lilly & Company (2014), index 2 to Chu et al. (2007) and index 3 is linked to Satterwhite et al. (2010)

$$\frac{\mathrm{d}PTH}{\mathrm{d}t} = \frac{F}{V_d} \cdot k_a \cdot D - k_e \cdot PTH + \beta_{PTH} \tag{4}$$

where Eq. (3) describes the variation over time of the drug present in the subcutaneous tissue, whereas Eq. (4) represents the drug concentration in the central compartment. D is the dose administered (in µg), PTH is the drug concentration in the central compartment (in mol/L), and F is the bioavailability of the drug dose once absorbed. V_d is the volume of distribution of the central compartment (in litres) corresponding to a Caucasian population. This latter quantity represents the apparent volume of the compartment and is correlated with the population treated (Jambekhar and Breen 2012). Finally, β_{PTH} is the endogenous PTH production term assumed to be constant and estimated from the relation $\beta_{PTH} = PTH_{baseline} \cdot k_e$ in order to remain constant a baseline PTH concentration. Note that the latter relation may change in pathologies such as hyperparathyroidism or hypoparathyroidism.

The present system of ODEs has been solved in MATLAB using an implicit, multi-step, variable-order, stiff solver (i.e., ode45). The solution for the (central compartment) PTH concentration for a 20 µg injection in a PMO population is shown in Fig. 1 (blue line). Model results are in good agreement with the experimental data of Satterwhite et al. (2010). The peak concentration is reached after 29 min, following a 20 µg subcutaneous injection, and returns to baseline after 4 h. Furthermore, we also compared our PK model results with experimental data from a healthy Asian population (Chu et al. 2007) and found again a good match between simulation results and experiments (see "Appendix 1" for details).

Note that the PTH dose enters the PK model of PTH(1-34) as a linear absorption term, in Eq. (3), which means that one can simply modify the initial dose in the ODEs based on the commonly used administrated dose, i.e. 10, 20 or 40 µg

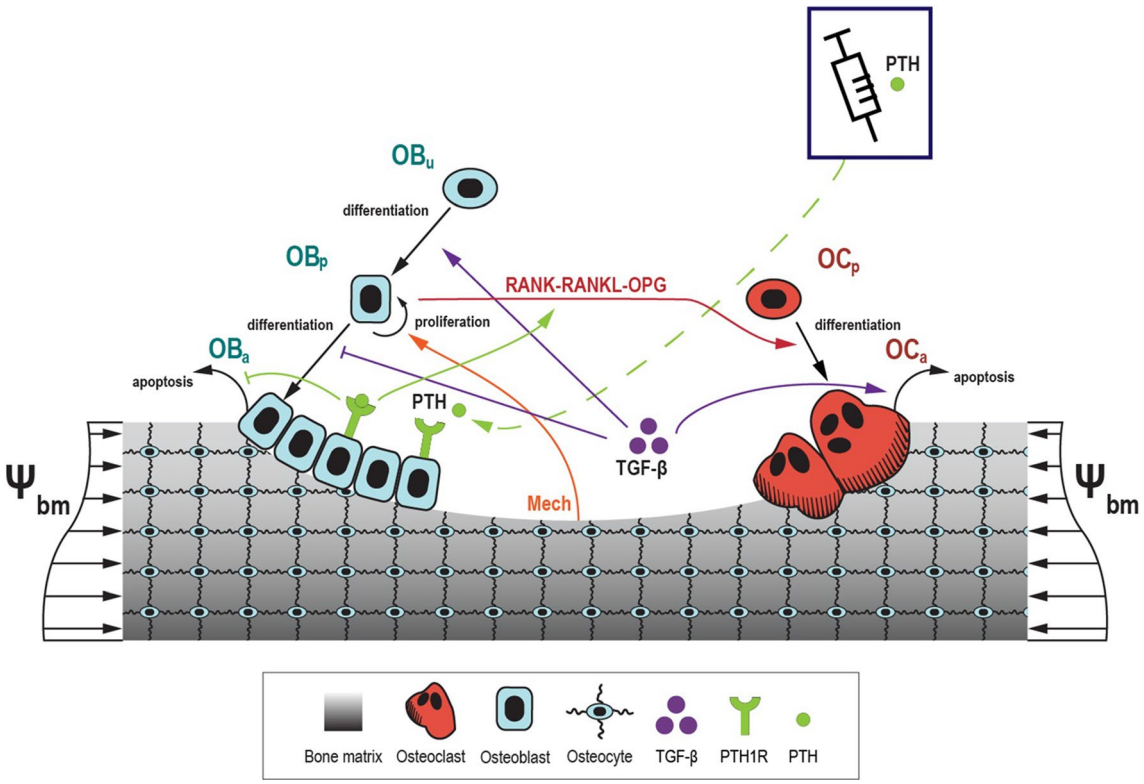

Fig. 2 Schematic illustration of the BCPM and its regulatory mechanisms implied in bone remodelling. RANK-RANKL-OPG pathway, TGF-β (Pivonka et al. 2013), PTH and osteocyte's mechanical feedback actions on the BCPM are shown by lines and arrows. Subcutaneous intermittent injection of PTH regulates osteoblast apoptosis and RANKL/OPG ratio

subcutaneous injection. All other parameters are assumed constant.

2.2 Bone cell population model (BCPM) accounting for dual action of PTH

In this paper, we used the bone cell population model introduced and described by Pivonka and co-workers (Trichilo et al. 2019; Scheiner et al. 2013; Pivonka et al. 2008, 2010). Effects of PTH on human interstitial bone (i.e. intracortical and trabecular) are exerted by changing bone turnover and bone remodelling balance. Indeed, two cell populations are known to govern the remodelling process. Osteoclasts are derived from hematopoietic stem cells and resorb the bone matrix, while osteoblasts are derived from mesenchymal stem cells and form the bone matrix. Finally, osteocytes are cells within the bone matrix and responsible for bone response to mechanical stimulus. The employed BCPM is schematically shown in Fig. 2.

As in previous bone cell population models (BCPMs), we assume a constant concentration of uncommitted osteoblasts (OB_u) and osteoclast precursors (OC_p). Consequently, the state variables in our model are osteoblast precursor cells (OB_p), active osteoblasts (OB_a) and active osteoclasts (OC_a). The concentrations of OB_p, OB_a and OC_a can be expressed as cell balance equations and lead to the following system of 3 ordinary differential equations (ODEs):

$$\frac{\mathrm{d}OB_p}{\mathrm{d}t} = D_{OB_u} \cdot \pi^{TGF\text{-}\beta}_{act,OB_u} \cdot OB_u + P_{OB_p} \cdot \pi^{mech}_{act} \cdot OB_p - D_{OB_p} \cdot \pi^{TGF\text{-}\beta}_{rep,OB_p} \cdot OB_p \tag{5}$$

$$\frac{\mathrm{d}OB_a}{\mathrm{d}t} = D_{OB_p} \cdot \pi^{TGF\text{-}\beta}_{rep,OB_p} \cdot OB_p - A_{OB_a} \cdot H^{-}_{PTH} \cdot OB_a \tag{6}$$

$$\frac{\mathrm{d}OC_a}{\mathrm{d}t} = D_{OC_p} \cdot \pi^{RANKL}_{act} \cdot OC_p - A_{OC_a} \cdot \pi^{TGF\text{-}\beta}_{act,OC_a} \cdot OC_a \tag{7}$$

where D_{OB_u}, D_{OB_p}, D_{OC_p} indicate differentiation rates of OB_u, OB_p and OC_p, respectively. A_{OB_a} and A_{OC_a} are apoptosis rates of OB_a and OC_a. Finally, P_{OB_p} is the proliferation rate of osteoblast precursor cells (OB_p). The various cell populations are linked via various regulatory factors: $\pi^{TGF\text{-}\beta}_{act,OB_u}$, $\pi^{TGF\text{-}\beta}_{rep,OB_p}$ and $\pi^{TGF\text{-}\beta}_{act,OC_a}$ represent activator and repressor functions related to the binding of TGF-β to its receptors. Similarly, π^{RANKL}_{act} stands for the activator function linked to RANK-RANKL-OPG binding. π^{mech}_{act} is an activator function linked to osteocyte mechanical feedback. The latter is described in more detail in Sect. 2.2.1. Parameters used to calibrate the PK model are detailed in Table 1.

The dual action of PTH is incorporated into the model via two regulatory functions: catabolic action of PTH is incorporated as in previous BCPM (Trichilo et al. 2019), i.e. via π^{RANKL}_{act}, while the anabolic action of PTH is incorporated via regulating the apoptosis rate A_{OB_a}. The latter quantity is regulated via intracellular signalling and is described by sigmoidal (repressor) function $H^{-}_{PTH} = f(Bcl{-}2)$ (see Sect. 2.2.2 for details). All functional relations describing receptor–ligand binding reactions are described in Trichilo et al. (2019).

Finally, we link bone cell biology of remodelling with mechanical aspects of bone via formulating an evolution equation of the *BV/TV* as a function of active osteoblasts and osteoclasts (Pivonka et al. 2008):

$$\frac{\mathrm{d}BV/TV}{\mathrm{d}t} = k_{form} \cdot OB_a - k_{res} \cdot OC_a \tag{8}$$

In Eq. (8), k_{form} and k_{res} represent the osteoblast formation rate and osteoclast resorption rate. The latter quantities are considered constant. Note that k_{form} can be obtained from the literature (Pivonka et al. 2013), while k_{res} is calculated based on assuming remodelling balance (i.e. homeostasis). Aiming at this later, we set the left-hand side of Eq. (8) to zero. This delivers $k_{res} = k_{form} \cdot OB_a(t_0)/OC_a(t_0)$.

Here we consider bone tissue as a two-phase composite material made of extravascular bone matrix (*BV/TV*) with vascular pores $(1 - BV/TV)$ in between (Scheiner et al. 2013; Pivonka et al. 2008, 2013), defined on a typical representative volume element (RVE). Initial $BV/TV(t_0)$ is chosen based on experimental data of a particular bone. For example, typical trabecular bone of the lumbar spine has a bone volume fraction of 8.5%, i.e. $BV/TV = 0.085$. In the next subsection, we use a micromechanical model of bone stiffness to calculate the strain energy density in the bone matrix. The latter quantity is used to formulate mechanical feedback on bone remodelling.

2.2.1 Mechanobiological feedback and physiological loading

The computational model of the PTH rat model developed in Trichilo et al. (2019) assumed that bone adaptation due to mechanical loading takes place at longer timescales (i.e. 2–3 weeks and above) compared to the timescale that investigated changes of *BV/TV* due to different doses of PTH (i.e. 1 week). Consequently, the latter model neglected the influence of mechanical feedback on *BV/TV*. For human drug interventions, typical timescales investigated are 12–24 months and, consequently, taking into account mechanical feedback is essential. Here, we follow the approach taken by Scheiner et al. (2013) and use the strain energy density in the bone matrix as a mechanical feedback quantity. This scalar quantity is sensed by osteocytes which then regulate anabolic and catabolic bone remodelling

responses. For completeness of the current work, we provide a short description of the mechanical model below.

Estimation of the microscale (i.e. bone matrix) strain energy density (ψ_{bm}) is based on a continuum micromechanics framework in which millimetre-scale bone material is represented as extravascular material with embedded cylindrical pores. This micromechanical model of bone delivers a so-called concentration relation between the macroscopic strains of a millimetre-sized RVE of bone (generated by macroscopic loading of the tissue), and the microscopic strain $\boldsymbol{\varepsilon_{bm}}$ induced at the level of the extravascular matrix hosting the osteocytes. Using this formulation, the microscopic strain energy density of the bone matrix ψ_{bm} can be expressed as a function of the macroscopic stress tensor $\boldsymbol{\Sigma}$, the bone matrix stiffness tensor $\mathbb{C}_{bm}$ and the bone volume fraction BV/TV (Pivonka et al. 2013):

$$\psi_{bm} = f(\boldsymbol{\Sigma}, \mathbb{C}, BV/TV) \tag{9}$$

The reader is referred to Scheiner et al. (2013) for the general mathematical specification of ψ_{bm} and a detailed presentation of the homogenization procedure. In the present paper, we specify the transversely isotropic bone matrix stiffness tensor $\mathbb{C}_{bm}$ according to human femur data obtained by ultrasonic tests (Ashman et al. 1984; Fritsch and Hellmich 2007):

$$\mathbb{C}_{bm} = \begin{pmatrix} 18.5 & 10.3 & 10.4 & 0 & 0 & 0 \\ 10.3 & 20.8 & 11.0 & 0 & 0 & 0 \\ 10.4 & 11.0 & 28.4 & 0 & 0 & 0 \\ 0 & 0 & 0 & 12.9 & 0 & 0 \\ 0 & 0 & 0 & 0 & 11.5 & 0 \\ 0 & 0 & 0 & 0 & 0 & 09.3 \end{pmatrix} \text{ GPa} \tag{10}$$

Using this micromechanical model of bone, we can compute the bone matrix strain energy density ψ_{bm}, and so formulate the biomechanical feedback. Catabolic feedback is accounted using an external RANKL production term, P_{RANKL}, by precursor osteoblasts which modulates the RANK-RANKL-OPG signalling pathway (Scheiner et al. 2013):

$$P_{RANKL} = \begin{cases} \kappa(1 - \frac{\psi_{bm}}{\psi_{bm}(t_0)}), & \psi_{bm} < \psi_{bm}(t_0) \\ 0, & \psi_{bm} \geq \psi_{bm}(t_0) \end{cases} \tag{11}$$

where κ is a parameter which represents the strength of the biomechanical feedback on catabolic bone response and $\psi_{bm}(t_0)$ is the strain energy density (SED) at the initial time point which is considered a homeostatic state.

Negative feedback is achieved for cases when the current SED is lower than the initial SED. For this case, P_{RANKL} increases linearly and leads to a higher π_{act}^{RANKL} value and, therefore, a higher differentiation of precursor osteoclast.

On the other hand, a mechanical overuse causes no catabolic action by the current biomechanical feedback, i.e. $P_{RANKL} = 0$. The biomechanical feedback accounting for bone formation is assumed to act on the proliferation of osteoblast precursor cells. The latter can be expressed in the form of an activator function, defined as:

$$\Pi_{act,OB_p}^{mech} = \begin{cases} \check{\Pi}_{act,OB_p}^{mech}, & \psi_{bm} < \psi_{bm}(t_0) \\ \check{\Pi}_{act,OB_p}^{mech}[1 + \lambda(\frac{\psi_{bm}}{\psi_{bm}(t_0)} - 1)], & \psi_{bm}(t_0) < \psi_{bm} < \psi_{bm}^{*} \\ 1, & \psi_{bm}^{*} < \psi_{bm} \end{cases} \tag{12}$$

where λ is a parameter which represents the strength of the biomechanical feedback on anabolic bone response, $\check{\Pi}_{act,OB_p}^{mech}$ is the minimum value of Π_{act,OB_p}^{mech} and is set to be equal to 1/2 in this study and ψ_{bm}^{*} is the minimum SED which leads to a maximum anabolic response $\Pi_{act,OB_p}^{mech} = 1$.

Moreover, we aimed to create a bone site-specific model as teriparatide presents various anabolic effects depending on the targeted bones (Leder et al. 2014). Hence, in the present model, bone sites were characterized by their initial bone volume fraction $BV/TV(t_0)$. Indeed, bone turnover and remodelling are different in different bones such as differently dense trabecular bone. For the purpose of this study, we used two bone sites which are the femoral neck and the lumbar spine with a $BV/TV(t_0)$ equal to, respectively, 25% and 8.5% (Hildebrand et al. 1999; Nazarian et al. 2007). We further assumed the existence of a physiological loading for each bone site which corresponds to the mechanical stress inducing a steady state of bone remodelling which is used to calculate $\Psi_{bm}(t_0)$. Based on estimates proposed by Frost, we set the physiological loading such as to reach the uniaxial bone strain ε_{33} of 800 $\mu\varepsilon$ (Frost 1983). By the use of Eq. (9), we are able to calculate a uniaxial longitudinal physiological stress Σ_{33} for a particular bone volume fraction, which we can introduce into $\boldsymbol{\Sigma}$ (where $\Sigma_{i,j} = 0$ for $(i,j) \neq (3,3)$). Hence, we computed a physiological stress of 11 MPa for the femoral neck and of 3 MPa for the lumbar spine. On the one hand, in case of a mechanical disuse, we decrease the mechanical loading, represented by Σ_{33}, by 20%. On the other hand, in case of a mechanical overuse, we increase the mechanical loading Σ_{33} by 20% (compared to physiological/habitual loading). We chose the latter value as in Scheiner et al. (2013) and Martin et al. (2019). This value is chosen rather arbitrarily as for any in vivo situation the reduction of physical activity would depend on the severity of the sustained injury and the healing duration, i.e. once full physical activity is regained.

2.2.2 Regulation of osteoblast apoptosis via PTH

In Sect. 2.1, we derived an expression for the serum PTH concentration as a function of external PTH dosing using a one-compartment PK model. As indicated in the introduction, a major effect of intermittent PTH is to reduce osteoblast apoptosis via modulating Bcl-2 transcription. Below we summarize a computational model of intracellular Bcl-2 regulation as a function of PTH administration. This model follows the developments presented previously (Trichilo et al. 2019; Peterson and Riggs 2010). Following PTH binding to its receptor PTH1R on osteoblastic cells, productions of Runt-related transcription factor 2 (Runx2) and phosphorylated cAMP response element-binding protein (pCREB) are differentially regulated (Peterson and Riggs 2010). Degradation of Runx2 is rapidly enhanced after intermittent PTH administration, whereas pCREB production is slowly increased upon intermittent PTH administration. Finally, these two regulatory factors drive the transcription rate of Bcl-2, an anti-apoptotic factor, and this transcription is assumed to follow intermediate dynamics modelled as the product of Runx2 and pCREB concentrations. The changes in concentration of the three regulatory factors can be described by the following three ODEs (Trichilo et al. 2019; Peterson and Riggs 2010):

$$\frac{\mathrm{d}Runx2}{\mathrm{d}t} = \beta_{Runx2} - Deg_{Runx2} \cdot H^{+}_{PTH,Runx2} \cdot Runx2 \tag{13}$$

$$\frac{\mathrm{d}pCREB}{\mathrm{d}t} = \beta_{pCREB} \cdot H^{+}_{PTH,pCREB} - Deg_{pCREB} \cdot pCREB \tag{14}$$

$$\frac{\mathrm{d}Bcl\text{-}2}{\mathrm{d}t} = \beta_{Bcl\text{-}2} \cdot Runx2 \cdot pCREB - Deg_{Bcl\text{-}2} \cdot Bcl\text{-}2 \tag{15}$$

where $Runx2$, $pCREB$ and $Bcl\text{-}2$ represent the (active osteoblast) intracellular concentration of Runx2, pCREB and Bcl-2, respectively. β_{Runx2}, β_{pCREB}, $\beta_{Bcl\text{-}2}$ stand for the production rate of Runx2, pCREB and Bcl-2, respectively, and Deg_{Runx2}, Deg_{pCREB}, $Deg_{Bcl\text{-}2}$ the degradation rate of Runx2, pCREB and Bcl-2, respectively. $H^{+}_{PTH,Runx2}$ and $H^{+}_{PTH,pCREB}$ are the H regulatory functions driven by the PTH dosing pattern, which, respectively, regulate the degradation rate of Runx2 and the production rate of pCREB. The sigmoidal shape of these H functions are described in Peterson and Riggs (2010) and is also used to model the indirect effect of PTH on the active osteoblast apoptosis rate, shown as follows:

$$H^{-}_{PTH} = \alpha_{A_{OB_a}} - \frac{(\alpha_{A_{OB_a}} - \rho_{A_{OB_a}}) \cdot Bcl\text{-}2^{\gamma_{A_{OB_a}}}}{\delta^{\gamma_{A_{OB_a}}}_{A_{OB_a}} + Bcl\text{-}2^{\gamma_{A_{OB_a}}}} \tag{16}$$

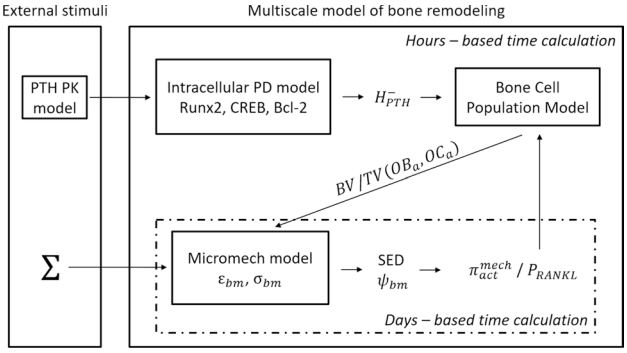

Fig. 3 Schematic representation of the algorithmic formulation implemented in our model. The model is driven in the following way: (1) external stimuli consist of PTH intermittent dosing (Sect. 2.1) and mechanical stress (Σ); (2) based on the mechanical stimuli, Ψ_{bm} is computed first and kept constant for Δ_t; (3) based on the PTH intermittent dosing stimuli, intracellular responses are computed (Sect. 2.2.2) and drive the active osteoblast apoptosis rate via the H^{-}_{PTH} function; (4) BCPM is simulated for Δ_t (Sect. 2.2) and returns the last *BV/TV* value to the micromech model which closes the feedback loop. Σ is the macroscopic stress tensor acting on the bone RVE

$\alpha_{A_{OB_a}}$, $\rho_{A_{OB_a}}$ are, respectively, the maximum and the minimum reached by the regulatory function, $\gamma_{A_{OB_a}}$ set its steepness and $\delta_{A_{OB_a}}$ is the potency of the H function. By utilizing Eq. (16), we can formulate the dependence of the osteoblast apoptosis rate on PTH as:

$$A_{OB_a}(PTH) = A_{OB_a}(t_0) \cdot H^{-}_{PTH} \tag{17}$$

where $A_{OB_a}(t_0)$ is the apoptosis rate of active osteoblasts in homeostasis.

2.3 Algorithmic model formulation

One can see in Fig. 3 the way we implemented the model's algorithm. The latter is composed of two distinct phases which, respectively, consist of our PK/PD PTH model combined with the BCPM and of our mechanical feedback block. Beginning with a time-dependent PTH concentration and a BCPM steady state, we resolve the ODEs on an hour-based time as the intra- and extracellular pathways are evolving quickly. On the other hand, the mechanical feedback is calculated on a diurnal time-scale.

We tried different values for the time between each update of the mechanical feedback, going from months to one single day. As a result, we decided to fix an updating period for the mechanical feedback at 3 days, which means that every 3 days we calculate the new values for Π^{mech}_{act,OB_p} and P_{RANKL} with the current *BV/TV* and the constant stress tensor Σ. We chose the above updating period as it appears low enough to get a nearly continuous response and did not have a big impact on

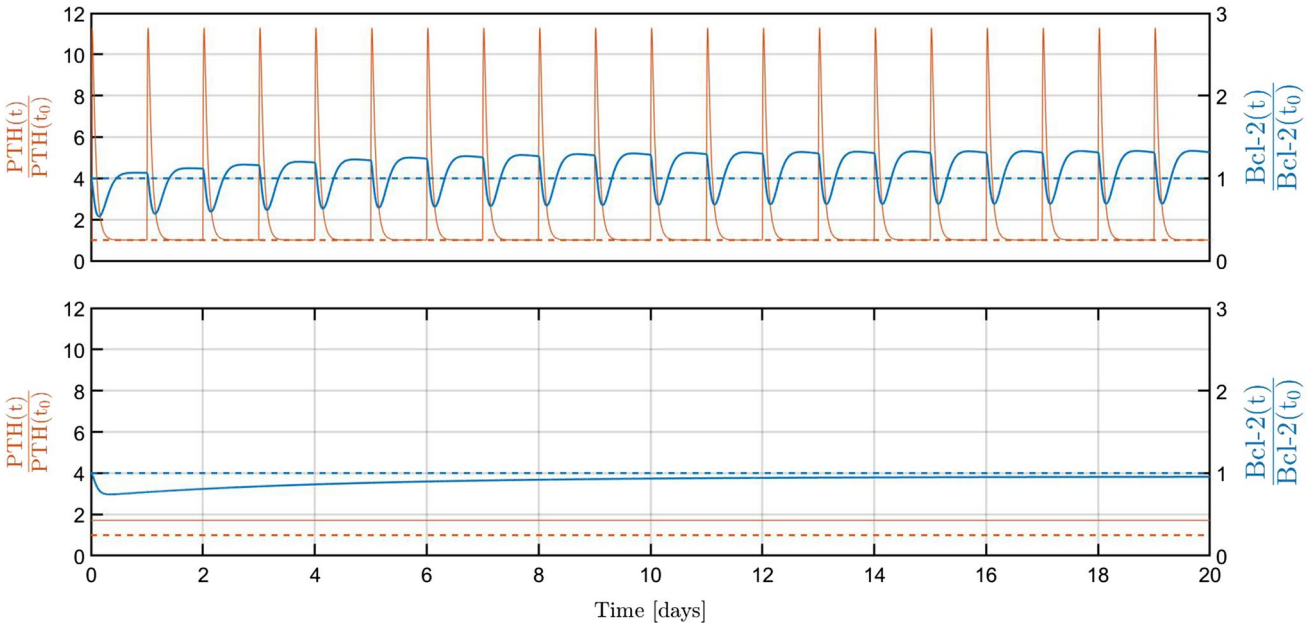

Fig. 4 Intracellular model regulating osteoblast apoptosis: evolution of the normalized concentrations of PTH (PK model) and Bcl-2 (PD model), resulting from Runx2 and CREB proteins' concentration changes. Cases of intermittent daily injections of 20 µg of PTH (top) and of continuous administration corresponding to a 1.7-fold the baseline concentration of PTH (bottom) are shown

the computational time compared to the hours-based resolution time of the BCPM.

All model parameters are presented in "Appendix 3".

3 Model calibration and validation

This section deals with the description of the model calibration based on a single set of experimental data, i.e. the data of *BV/TV* at the hip (i.e. femoral neck) of a PMO population undergoing 2-year treatment with 20 µg/day PTH dosing (Leder et al. 2014). Note that model validation is subsequently performed on different PTH dosing regimens and bone sites.

In Fig. 4, we can see how PTH serum concentration drives, indirectly, the concentration changes of the protein Bcl-2. Bcl-2 is directly driven by the concentrations of Runx2 and pCREB. Note that Runx2 and pCREB exhibit different response times to intermittent changes of PTH, as explained in Sect. 2.2.2, and their dynamics can be observed in Trichilo et al. (2019). In the intermittent administration case (cf. Fig. 4-Top), Bcl-2 reaches (on average) about 1.2-fold of its initial value at day 15. The latter value drives the anabolic bone response via the H function of Eq. (16). For the continuous PTH administration case (cf. Fig. 4-Bottom), a constant PTH injection is selected leading to a 1.7-fold increase in PTH serum concentration. The latter value was selected as it represents the same daily dose compared to daily 20 µg injections of PTH. For the continuous case, the Bcl-2 concentration at steady state is slightly lower than the initial value. More details can be found on the H function driving the OB_a apoptosis rate in "Appendix 2."

Model simulations provide the evolution of *BV/TV* (see Eq. (8)). We note that changes in bone mass during PTH treatment are reported either in terms of *BV/TV* or as BMD values. Here we are concerned with relative changes of bone mass, i.e. bone density gain (BDG); hence, we can use either BMD or *BV/TV* data for comparative purposes. Therefore, in order to compare our model results with the literature, we computed the bone density gain (BDG) as a percentage at an instant t using the following equation:

$$\mathrm{BDG} = \frac{BV/TV(t) - BV/TV(t_0)}{BV/TV(t_0)} \tag{18}$$

where $BV/TV(t_0)$ is the time when treatment commenced.

Following previous modelling approaches, we simulate PMO by administering a constant external dose of RANKL, P^d_{RANKL} (Trichilo et al. 2019; Pivonka et al. 2008, 2010; Scheiner et al. 2014). This parameter was computed such that a bone resorption of approximately 0.45% and 1.16% was obtained after 1 year, at the femoral neck and at the lumbar spine, respectively (Harris and Dawson-Hugues 1992) (cf. Table 3). Due to mechanical feedback, the *BV/TV* curve reaches a horizontal plateau after a characteristic time. This time depends on the strength of the anabolic mechanical feedback (λ). Note that the value of λ was chosen the same as in Scheiner et al. (2013), while the catabolic parameter (κ)

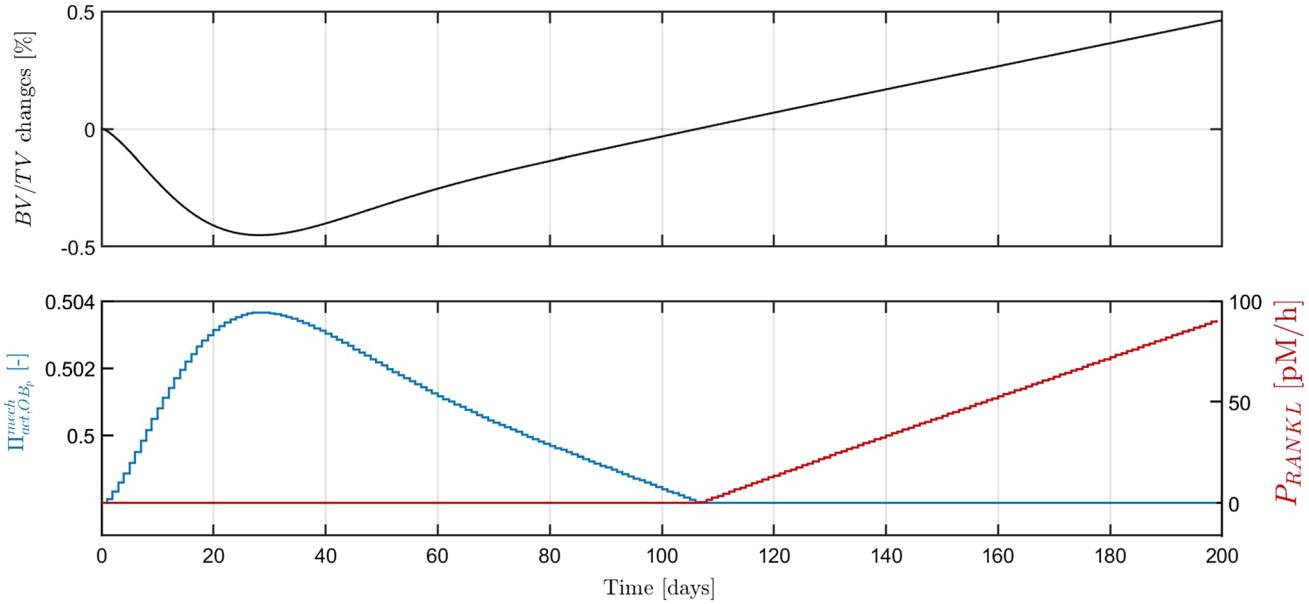

Fig. 5 Mechanistic PK-PD model of PMO treatment: relative *BV/TV* changes versus time at the femoral neck during daily PTH injections of 20 µg (top) and mechanical feedback quantities (bottom)

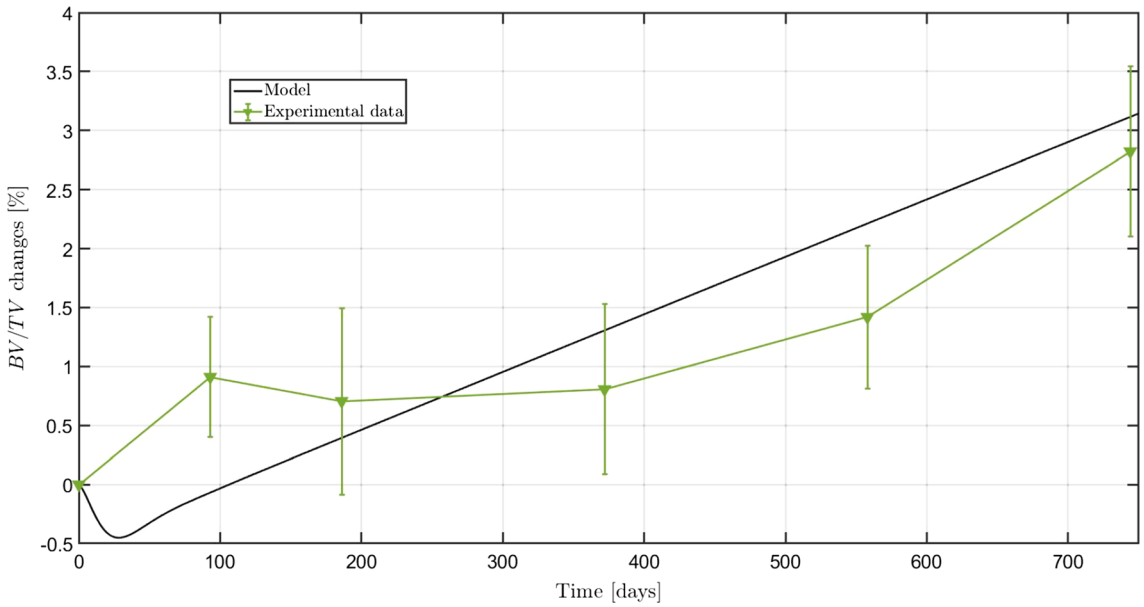

Fig. 6 Relative changes in *BV/TV* at femoral neck with 20 µg daily PTH injections over 2-year treatment—model calibrated (black line) on experimental data (BDG from Leder et al. (2014) at femoral neck with 20 µg daily injections (green line and bars)

was reduced from 10^5 to 10^4 in the current model indicating a more moderate feedback.

Figure 5 (top) shows the BDG (at the femoral neck) over time for the 20 µg intermittent PTH administration in PMO. Intermittent PTH injections initially lead to a catabolic response during the first 25 days before the BDG increases quasi-linearly. Figure 5 (bottom) shows the actions of the mechanical feedback quantities (see Eq. (11) and (12)). During the first 110 days, characterized by negative values of BDG, the anabolic pathway is activated. The catabolic pathway of the mechanostat feedback is activated once the

Table 2 Model parameters chosen for the mechanical feedbacks λ and κ, the postmenopausal osteoporosis simulation P^{d}_{RANKL} and the indirect effect of PTH on osteoblast apoptosis rate via the H^{-}_{PTH} function

Parameter	Description	Value
λ	Anabolic constant	125
κ	Catabolic constant	10^4
P^{d}_{RANKL}	RANKL external injection	1.25 pM h^{-1}
$\alpha_{A_{OB_a}}$	H^{-}_{PTH} maximum	1.2
$\rho_{A_{OB_a}}$	H^{-}_{PTH} minimum	0.8
$\gamma_{A_{OB_a}}$	H^{-}_{PTH} steepness	5.6
$\delta_{A_{OB_a}}$	H^{-}_{PTH} potency	100 pM

bone volume fraction becomes larger than its initial value, i.e. from 110 days onwards (Fig. 6).

Table 2 summarizes the model parameters which have been optimized based on available experimental data. In Table 3, experimental data reported by various research groups are summarized together with in silico simulation results using our model. Harris et al. provide reference data for BDG in PMO without treatment (both at femoral neck and lumbar spine) (Harris and Dawson-Hugues 1992). Leder et al. 2014 report on BDG over a 2-year period with daily 20 µg PTH treatment (Leder et al. 2014). Neer et al. (2001) report also on BDG over a 2-year period with daily 20 µg PTH treatment (Neer et al. 2001). Note that the standard deviations of the experimental data in Neer et al. 2001 are quite large compared to Leder et al. (2014).

Figure 7 shows the BDG at the femoral neck over a 2-year period with daily 20 µg PTH injections. One can see that

Table 3 Comparison between simulated relative *BV/TV* changes obtained with the present model and experimental data from the literature: PMO control over 1 year (Harris and Dawson-Hugues 1992) and 2 years (Neer et al. 2001) and with treatment of daily 20 µg PTH injections over 2 years (Neer et al. 2001; Leder et al. 2014)

	Lumbar spine		Femoral neck	
	Control	PTH 20 µg	Control	PTH 20 µg
Leder et al. (2014) 2 years	–	9.4 ± 1.13%	–	2.82 ± 0.72%
Neer et al. (2001) 2 years	1.1 ± 5.5%	9.7 ± 7.4%	− 0.7 ± 5.4%	2.8 ± 7.4%
Harris and Dawson-Hugues (1992) 1 year	− 1.16 ± 2.15%	–	− 0.45 ± 0.88%	–
Model simulation	− 0.97% (1 year)	–	− 0.44% (1 year)	–
	− 1.09% (2 years)	8.66%	− 0.60% (2 years)	3.14%

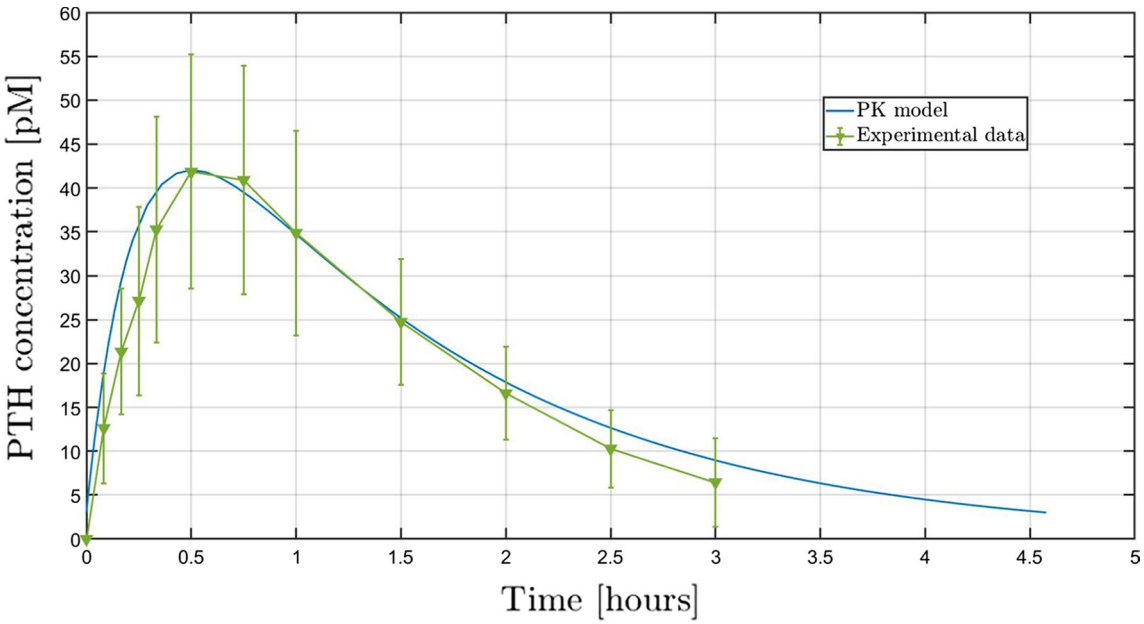

Fig. 7 Serum PTH concentration against time. Blue line shows the PK model simulation. Green line and bars represent experimental data from a 20 µg single injection of teriparatide in an Asian PMO population (Chu et al. 2007)

Table 4 Comparison between the effects of different PTH doses (10, 20, 40 µg) on relative *BV/TV* changes in the case of daily PTH injections over 2 years at lumbar spine and femoral neck sites

	Lumbar spine			Femoral neck		
	PTH 10 µg	PTH 20 µg	PTH 40 µg	PTH 10 µg	PTH 20 µg	PTH 40 µg
Model simulation (PMO)	1.97%	8.66%	17.33%	0.68%	3.14%	6.16%

Table 5 Comparison between the effects of different bone mechanical use levels on relative *BV/TV* changes after two years: control (physiological stress set in Sect. 2.2.1), disuse (20% below physiological stress), overuse (20% over physiological stress) in function of different bone locations (LS and FN) and different PTH treatment: PMO population with (PTH 20 µg) or without (control) daily injections of PTH

	Lumbar spine			Femoral neck		
	Disuse	Control	Overuse	Disuse	Control	Overuse
Control (%)	− 6.89	− 1.09	14.08	− 2.61	− 0.60	7.53
PTH 20 µg (%)	5.21	8.66	21.77	1.87	3.14	11.81

the simulation results in the first 100 days deviate from the experimental data, but that from 200 days onwards the in silico model replicates the trend of experimentally observed BDG in Leder et al. (2014).

Finally, Table 3 summarizes how the in silico results of our model are in good agreement with the experimental data available in the literature, regarding skeletal sites or PTH treatment. Moreover, it is important to notice that those results were obtained with only one set of parameters which were calibrated on the femoral neck. Indeed, only an initial site-dependent *BV/TV* and a physiological stress Σ will modulate the results. Simulated BDG values for lumbar spine are considered as a result as we did not calibrate our model with experimental data at this particular site.

4 Results

After model calibration, we now investigate whether the model is able to predict other experimental conditions related to PTH treatment of PMO. Firstly, we investigate if the model is able to predict variation in PTH dose and bone site-specific differences in PTH treatment of PMO. Then, we investigate the combined action of PTH and mechanical loading on a PMO population.

4.1 PTH doses and bone site specificity

We first vary the most commonly injected PTH dose (20 µg PTH) to a lower and higher dose, respectively, to assess drug efficacy. To do this, we use the PK model and simulate daily injections of PTH at 10 and 40 µg, respectively. Simulation results are summarized in Table 4. One can see that BDG at 2-year PTH treatment is always higher in the lumbar spine compared to the femoral neck. Moreover, there is a nonlinear increase in BDG with dose. For example, at the lumbar spine, a two-fold dose increase from 10 to 20 µg leads to an eight-fold increase in BDG. Furthermore, a four-fold dose increase from 10 to 40 µg leads to a more than 20-fold increase in BDG. We note that the simulation values of BDG for the 40 µg dose are 17.33% at the lumbar spine and 6.16% at the femoral neck, which are in good agreement with data from the literature. Indeed, Neer et al. (2001) tested a 40 µg daily PTH dose in a PMO population and found BDG of 13.7 ± 9.7% in the lumbar spine and 5.1 ± 6.7% in the femoral neck.

4.2 Combined PTH and mechanical loading

As mentioned in the Methods section, our model is also able to simulate physical loading, i.e. by changing the mechanical forces acting on bone. Indeed, we represented physical activity by a uniaxial tissue scale stress state (Σ), which we reduced or increased by 20% to simulate, respectively, a disuse or an overuse mechanical loading case. Table 5 summarizes the simulated results.

Note that the control values of BDG are for non-treated PMO population and for 20 µg PTH daily injections at two years. The first line in Table 5 shows the effect of the mechanical feedback only on BDG. Indeed, one can see that disuse superimposed on PMO decreases BDG, while overloading can offset the bone loss due to PMO given a positive value of BDG. Bone loss and gain are site specific with the lumbar spine being more responsive compared to femoral neck, i.e., − 6.89% (disuse) and 14.08% (overuse) at lumbar spine.

The second line in Table 5 shows combined action of mechanical disuse/overuse loading and a 20 µg daily PTH injections at two years. Despite mechanical disuse, BDG is positive (5.21% for lumbar spine and 1.87% for femoral neck). However, PTH's anabolic response is ablated compared to control (8.66% for lumbar spine and 3.14% for femoral neck). In the case of high physical activity combined with PTH treatment, one clearly observes a synergistic increase in BDG, i.e. 21.77% at the lumbar spine. Furthermore, at the femoral neck a 11.81% BDG is observed.

5 Discussion

Among the several mechanisms proposed to drive the anabolic response of intermittent PTH, we implemented the effect of PTH on osteoblast apoptosis rate. The latter effect was simulated via an intracellular signalling model taking into account three regulatory factors, i.e. Runx2, pCREB and Bcl-2. The simulation results (cf. Fig. 4) indicate that for 20 µg intermittent PTH injections, the Bcl-2 concentration is increased by around 1.2-fold in average which leads to an approximate 1.15-fold reduction of the osteoblast apoptosis rate (A_{OB_a}). Note that the catabolic bone response of the BCPM is mostly due to the action of RANKL and to a much lesser extent due to the small increase in Bcl-2 concentration in the intracellular model.

The experimental BMD data of intermittent PTH treatment of PMO indicate that different bone sites respond differently to hormonal changes and therapy with the lumbar spine showing a larger responsiveness compared to the femoral neck (Leder et al. 2014). Note that in PMO the lumbar spine exhibits a larger bone loss compared to the femoral neck (see control data Table 3). BDG is higher at lumbar spine compared to femoral neck after PTH treatment (see Table 3). One explanation for this behaviour is that different bone sites are characterized by different turnover rates and initial *BV/TV* values. In our BCPM, we can account for the changes in bone turnover by assigning different *BV/TV* values to different bone sites, while keeping bone cell numbers constant in the RVE. Hence, bone sites with lower $BV/TV(t_0)$ exhibit a higher bone turnover compared to sites with larger initial *BV/TV*. Another model feature which is crucial to replicate the experimental data is to adjust the (tissue scale) mechanical stress acting on the RVE. The latter was chosen based on the initial *BV/TV* and the constraint that the strain in the bone matrix was 800 µϵ. With these model features, it was possible to replicate all the experimental data listed in Table 3, using only the 20 µg PTH dose and the femoral neck as calibration values.

An important aspect of PK-PD modelling is to study drug efficacy. Varying the (intermittent) PTH dose clearly showed a nonlinear relationship between BDG and PTH dose, with higher doses leading to larger bone gains. While in the simulation results, we report on BDG changes for the highest dose of 40 µg, we also tested cases of higher doses which are not physiological meaningful and may have side effects. One model feature for higher doses is that due to mechanical feedback, there exists an upper limit of BDG. Increasing the dose beyond that limit does not lead to further BDG increase. We also note that the model was able to predict the experimentally reported BDG for the 40 µg PTH dose. Indeed, in the Neer et al. (2001), they also tested a 40 µg daily dose in a PMO population and found results of increased BMD of 13.7 ± 9.7% in the lumbar spine and 5.1 ± 6.7% in the femoral neck.

Based on the fact that several studies (both in humans and animal models) have reported that PTH and mechanical loading interact, we performed a parametric study of combining mechanical disuse and overuse scenarios with a 20 µg intermittent PTH treatment. Our simulation results indicate that mechanical disuse reduces the PTH anabolic bone response, while mechanical overuse enhances BDG. The combined effect of PTH and mechanical loading (i.e. 11.81% at the femoral neck) is larger than summation of the individual responses (i.e. addition of the individuals BDG of PTH and mechanical overuse equals 10.58% at the femoral neck). Similar results are obtained for the lumbar spine. While experimental data on humans investigating the combined action of PTH and mechanical loading are lacking, animal models suggest that a certain baseline activity of physiological loading is required for the anabolic PTH response (Sugiyama et al. 2008). Our model results indicate that mechanical disuse counteracts the effects of PTH, and consequently, subjects undergoing a PTH treatment should be encouraged to perform a baseline physiological exercise regimen (Sugiyama et al. 2008).

The last study presented in this paper deals with the effect of mechanical disuse on the effect of anabolic PTH stimuli. Experimental data from animal models indicate that the anabolic effect of PTH is reduced during periods of mechanical disuse. This phenomenon is commonly explained conceptually by the fact that mechanical disuse leads to a catabolic bone response and that superimposing the anabolic PTH effect leads to a reduced overall bone gain. In humans, the effect of mechanical disuse is equivalent to low physical mobility as occurring in elderly frail people. However, quantifying the effect of combined low physical mobility together with PTH treatment has been challenging. One major factor is the lack of a quantitative measure for physical activity.

6 Conclusions

To investigate the effects of PTH(1-34) treatment of PMO on bone mineral density, we developed a mechanistic PK/PD model. The PK model consists of a one-compartment model calibrated for a PMO population receiving daily subcutaneous PTH injections. This work is an extension of a previous model. This new model incorporates additional model features such as regulation of the osteoblast apoptosis rate based on an intracellular model and incorporation of a mechanical feedback. Based on our numerical simulations, the following conclusions can be made:

- Osteoblast apoptosis rate is an efficient regulator of anabolic bone response to intermittent PTH treatment.
- *BV/TV* gain is nonlinearly governed by PTH dose, with higher doses leading to larger *BV/TV* gains.
- *BV/TV* gain is bone site specific.
- Mechanostat feedback is essential to simulate site-specific bone responses.
- *BV/TV* gain from combined PTH and mechanical loading is larger than the individual response of each therapy alone.
- Mechanical disuse reduces the anabolic effects of PTH.

Our results indicate that the model is capable of replicating a variety of experimental data of PTH treatment of PMO and gives confidence that essential mechanisms in bone remodelling have been adequately captured. In the future, further testing of the model on complementary experimental data is required. In particular, application of the model to combined PTH and anti-resorptive treatment cases would be of interest.

Acknowledgements Mister Maxence Lavaill gratefully acknowledges the support by the Queensland University of Technology, in the framework of the Supervisor's PhD Scholarship Program.

Compliance with ethical standards

Conflict of interest The authors declare that they have no conflict of interest.

Appendix 1: PK model calibrated on an Asian population

Asian populations are usually lighter than Caucasian populations. This will have an influence on the created PK model. Indeed, the volume of distribution V_d represents the one-compartment model described in Sect. 2.1. We consider an average weight of 50 kg for an Asian osteoporotic female population (Lin et al. 2004). We deduce the volume of distribution from the average weight as $V_d = 1.7$ L/kg as the pharmacokinetics of PTH in humans is linear. Hence, we can simulate our PK model as we did previously in Sect. 2.1.

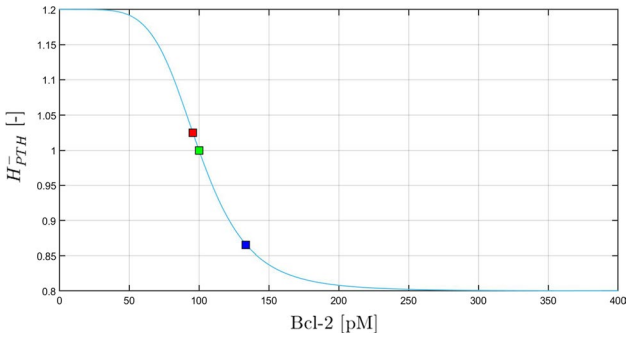

Fig. 8 H^-_{PTH} plot in function of Bcl-2 concentration—green square represents the baseline value when PTH is only endogenously produced, i.e. no external PTH injection. Red square represents the catabolic value corresponding to the continuous PTH administration from Fig. 4. Blue square represents the anabolic value corresponding to the intermittent 20 µg PTH injections from Fig. 4

Appendix 2: OB_a apoptosis rate H function

$$H^-_{PTH} = \alpha_{A_{OB_a}} - \frac{(\alpha_{A_{OB_a}} - \rho_{A_{OB_a}}) \cdot Bcl\text{-}2^{\gamma_{A_{OB_a}}}}{\delta^{\gamma_{A_{OB_a}}}_{A_{OB_a}} + Bcl\text{-}2^{\gamma_{A_{OB_a}}}} \tag{19}$$

The H function driving the OB_a apoptosis rate is important in our model as it will translate intracellular signal (Bcl-2 concentration) into a cell response and will be one of the major drivers of the dual response of PTH. We calibrated this function using the parameters shown in Table 2 such that $H^-_{PTH} = 1$ at the PTH concentration baseline (cf. Fig. 8, green dot). In the case of intermittent daily injections, the H^-_{PTH} will decrease the value of osteoblast apoptosis rate (red dot in Fig. 8), whereas continuous administration (cf. Fig. 4) will lead to a catabolic answer and therefore will increase apoptosis rate of OB_a by setting the H^-_{PTH} above 1 (blue dot in Fig. 8).

Appendix 3: Model parameters

See Table 6.

Table 6 Parameters governing the present PK/PD model

Parameter	Description	Value	Unit
K_{res}	Volume of bone matrix resorbed per osteoblast per hour	8.333	$(\text{pM h})^{-1}$
OB_u	Osteoblast progenitor concentration	10^{-3}	pM
OC_p	Osteoclast progenitor concentration	10^{-3}	pM
$OB_p(t_0)$	Osteoblast precursors baseline concentration	$1.005 \cdot 10^{-3}$	pM
$OB_a(t_0)$	Active osteoblast baseline concentration	5.021×10^{-3}	pM
$OC_a(t_0)$	Active osteoclast baseline concentration	1.005×10^{-4}	pM
$PTH(t_0)$	Endogenous PTH baseline concentration	3	pM
$TGF\text{-}\beta(t_0)$	*TGF-β* baseline concentration	1.005×10^{-4}	pM
$OPG(t_0)$	*OPG* baseline concentration	1.583×10^{4}	pM
$RANK(t_0)$	*RANK* baseline concentration	9.764	pM
$RANKL(t_0)$	*RANKL* baseline concentration	7.105×10^{-1}	pM
$OL(t_0)$	*OL* baseline concentration	11.247	pM
$KL(t_0)$	*KL* baseline concentration	2.367×10^{-1}	pM
D_{OB_u}	OB_u differentiation rate	2.916×10^{-2}	pM
D_{OB_p}	OB_p differentiation rate	6.917×10^{-3}	pM
D_{OC_p}	OC_p differentiation rate	8.75×10^{-2}	pM
P_{OB_p}	OB_p proliferation rate	1.758×10^{-3}	pM
A_{OB_a}	OB_a apoptosis rate	8.792×10^{-3}	pM
A_{OC_a}	OC_a apoptosis rate	2.354×10^{-1}	pM
α	*TGF-β* stored in the bone matrix	10^{-2}	pM
N_{RANK,OC_p}	Number of *RANK* per OC_p	10^{4}	–
$N_{RANKL,OB_p,max}$	Max number of *RANKL* per OB_p	2.7×10^{6}	–
OPG_{sat}	Max *OPG* concentration	2×10^{8}	pM
P^d_{RANKL}	*RANKL* external injection	1.25	pM h^{-1}
P^d_{OPG}	*OPG* external injection	0	$pM.h^{-1}$
P^d_{PTH}	*PTH* external injection	0	$pM.h^{-1}$
$P^d_{TGF\text{-}\beta}$	*TGF-β* external injection	0	pM h^{-1}
$Deg_{TGF\text{-}\beta}$	*TGF-β* degradation rate	8.333×10^{-2}	pM h^{-1}
Deg_{PTH}	*PTH* degradation rate	8.316	h^{-1}
Deg_{OPG}	*OPG* degradation rate	1.458×10^{-2}	h^{-1}
Deg_{RANKL}	*RANKL* degradation rate	4.167×10^{-1}	h^{-1}
Deg_{OL}	*OL* degradation rate	4.167×10^{-1}	h^{-1}
Deg_{KL}	*KL* degradation rate	8.750×10^{-2}	h^{-1}
Deg_{RANK}	*RANK* degradation rate	8.750×10^{-1}	h^{-1}
β_{OPG}	*OPG* production rate	6.792×10^{6}	h^{-1}
β_{RANKL}	*RANKL* production rate	7.00×10^{6}	h^{-1}
β_{PTH}	*PTH* production rate	24.948	h^{-1}
$K^{D,TGF\text{-}\beta}_{rep}$	Repressing constant related to *TGF-β* binding to its receptors on OB_p	1.750×10^{-4}	pM
$K^{D,TGF\text{-}\beta}_{act}$	Activating constant related to *TGF-β* binding to its receptors on OB_p	5.63×10^{-4}	pM
$K^{D,PTH}_{rep}$	Repressing constant related to *TGF-β* binding to its receptors on OB_p and OB_a	2.226×10^{-1}	pM
$K^{D,PTH}_{act}$	Activating constant related to *TGF-β* binding to its receptors on OB_p and OB_a	1.2	pM
$k_{r,OPG}$	$OPG - RANKL$ unbinding rate constant	4.167×10^{-1}	h^{-1}
$k_{f,OPG}$	$OPG - RANKL$ binding rate constant	8.33×10^{-4}	pM h^{-1}
$k_{r,RANK}$	$RANK - RANKL$ unbinding rate constant	7.08×10^{-4}	h^{-1}
$k_{f,RANK}$	$RANK - RANKL$ binding rate constant	3.00×10^{-3}	pM h^{-1}
$Runx2(t_0)$	*Runx*2 baseline value	10	pM
$CREB(t_0)$	*CREB* baseline value	10	pM

Table 6 (continued)

Parameter	Description	Value	Unit
$Bcl\text{-}2(t_0)$	*Bcl*-2 baseline value	100	pM
β_{Runx2}	*Runx*2 production rate constant	6.93	h^{-1}
β_{CREB}	*CREB* production rate constant	9.990×10^{-2}	h^{-1}
$\beta_{Bcl\text{-}2}$	*Bcl*-2 production rate constant	6.983×10^{-1}	h^{-1}
Deg_{Runx2}	*Runx*2 degradation rate constant	1	h^{-1}
Deg_{CREB}	*CREB* degradation rate constant	9.60×10^{-3}	h^{-1}
$Deg_{Bcl\text{-}2}$	*Bcl*-2 degradation rate constant	6.983×10^{-1}	h^{-1}
γ_{Runx2}	*Runx*2 response steepness	1	–
α_{Runx2}	*Runx*2 max response	2.563	–
ρ_{Runx2}	*Runx*2 min response	1.250×10^{-1}	–
δ_{Runx2}	*Runx*2 response potency	9.874	pM
γ_{CREB}	*CREB* response steepness	1	–
α_{CREB}	*CREB* max response	15.588	–
ρ_{CREB}	*CREB* min response	5.0×10^{-1}	–
δ_{CREB}	*CREB* response potency	95.195	pM
$\gamma_{A_{OB_a}}$	H^-_{PTH} response steepness	5.6	–
$\alpha_{A_{OB_a}}$	H^-_{PTH} max response	1.2	–
$\rho_{A_{OB_a}}$	H^-_{PTH} min response	0.8	–
$\delta_{A_{OB_a}}$	H^-_{PTH} response potency	100	pM
$\check{\Pi}^{mech}_{act,OB_p}$	Min value of the anabolic mechanical feedback	0.5	–
α	Strength of the anabolic mechanical feedback	1.25	–
κ	Strength of the catabolic mechanical feedback	10^{-4}	–
$t_{1/2}$	Half-life of PTH	1	h
$t_{C_{max}}$	Time to reach maximum concentration after injection	0.5	h
k_e	PTH elimination constant	0.693	h^{-1}
k_a	PTH absorption constant	4.38	h^{-1}
F	Bioavailability	0.95	–
V_d	Volume of distribution	110	L

References

Ashman RB, Cowin SC, Van Buskirk WC, Rice JC (1984) A continuous wave technique for the measurement of the elastic properties of cortical bone. J Biomech 17(5):349–361. https://doi.org/10.1016/0021-9290(84)90029-0

Bellido T, Ali AA, Plotkin LI, Fu Q, Gubrij I, Roberson PK, Weinstein RS, O'Brien CA, Manolagas SC, Jilka RL (2003) Proteasomal degradation of Runx2 shortens parathyroid hormone-induced anti-apoptotic signaling in osteoblasts. J Biol Chem 278(50):50259–50272. https://doi.org/10.1074/jbc.M307444200

Brent MB, Brüel A, Thomsen JS (2018) PTH (1-34) and growth hormone in prevention of disuse osteopenia and sarcopenia in rats. Bone 110(1):244–253. https://doi.org/10.1016/j.bone.2018.02.017

Canalis E (2018) Novel anabolic treatments for osteoporosis. Eur J Endocrinol 178(2):33–44. https://doi.org/10.1530/EJE-17-0920

Chu N, Li XN, Chen WL, Xu HR (2007) Pharmacokinetics and safety of recombinant human parathyroid hormone (1-34) (teriparatide) after single ascending doses in Chinese healthy volunteers. Pharmazie 62(11):869–871. https://doi.org/10.1691/ph.2007.11.7576

Dobnig H (2004) A review of teriparatide and its clinical efficacy in the treatment of osteoporosis. Expert Opin Pharmacother 5(5):1153–1162. https://doi.org/10.1517/14656566.5.5.1153

Eli Lilly & Company (2014) FORTEO teriparatide (rbe) injection—instruction guide

Ferrari S (2014) Future directions for new medical entities in osteoporosis. Best practice and research. Clin Endocrinol Metab 28(6):859–870. https://doi.org/10.1016/j.beem.2014.08.002

Fritsch A, Hellmich C (2007) 'Universal' microstructural patterns in cortical and trabecular, extracellular and extravascular bone materials: micromechanics-based prediction of anisotropic elasticity. J Theor Biol 244(4):597–620. https://doi.org/10.1016/j.jtbi.2006.09.013

Frost HM (1983) A determinant of bone architecture. Clin Orthop Relat Res 175(1):286–292. https://doi.org/10.1097/00003086-198305000-00047

Harris S, Dawson-Hugues B (1992) Rates of change in bone mineral density of the spine, heel, femoral neck and radius in healthy postmenopausal women. Bone Miner 17(1):87–95. https://doi.org/10.1016/0169-6009(92)90713-N

Hildebrand T, Laib A, Muller R, Dequeker J, Ruegsegger P (1999) Direct three-dimensional morphometric analysis of human cancellous bone: microstructural data from spine, femur, iliac crest,

and calcaneus. J Bone Miner Res 14(7):1167–1174. https://doi.org/10.1359/jbmr.1999.14.7.1167

Jambekhar SS, Breen PJ (2012) Extravascular routes of drug administration. Basic pharmacokinetics (chap 6), 2nd edn. Pharmaceutical Press, London, pp 105–126

Kostenuik PJ, Harris J, Halloran BP, Turner RT, Morey-Holton ER, Bikle DD (1999) Skeletal unloading causes resistance of osteoprogenitor cells to parathyroid hormone and to insulin-like growth factor-I. J Bone Miner Res 14(1):21–31. https://doi.org/10.1359/jbmr.1999.14.1.21

Langdahl B, Ferrari S, Dempster DW (2016) Bone modeling and remodeling: potential as therapeutic targets for the treatment of osteoporosis. Ther Adv Musculoskelet Dis 8(6):225–235. https://doi.org/10.1177/1759720X16670154

Leder BZ, Neer RM, Wyland JJ, Lee HW, Burnett-Bowie SAM, Finkelstein JS (2009) Effects of teriparatide treatment and discontinuation in postmenopausal women and eugonadal men with osteoporosis. J Clin Endocrinol Metab 94(8):2915–2921. https://doi.org/10.1210/jc.2008-2630

Leder BZ, Tsai JN, Uihlein AV, Burnett-Bowie SAM, Zhu Y, Foley K, Lee H, Neer RM (2014) Two years of denosumab and teriparatide administration in postmenopausal women with osteoporosis (The DATA extension study): a randomized controlled trial. J Clin Endocrinol Metab 99(5):1694–1700. https://doi.org/10.1210/jc.2013-4440

Lin YC, Wang MJJ, Wang EM (2004) The comparisons of anthropometric characteristics among four peoples in east Asia. Appl Ergon 35(2):173–178. https://doi.org/10.1016/j.apergo.2004.01.004

Martin M, Sansalone V, Cooper DM, Forwood MR, Pivonka P (2019) Mechanobiological osteocyte feedback drives mechanostat regulation of bone in a multiscale computational model. Biomech Model Mechanobiol 18(5):1475–14796. https://doi.org/10.1007/s10237-019-01158-w

Martínez-Reina J, Pivonka P (2019) Effects of long-term treatment of denosumab on bone mineral density: insights from an in-silico model of bone mineralization. Bone 125(1):87–95. https://doi.org/10.1016/j.bone.2019.04.022

Nazarian A, Muller J, Zurakowski D, Müller R, Snyder BD (2007) Densitometric, morphometric and mechanical distributions in the human proximal femur. J Biomech 40(11):2573–2579. https://doi.org/10.1016/j.jbiomech.2006.11.022

Neer RM, Arnaud CD, Zanchetta JR, Prince R, Gaich GA, Reginster JY, Hodsman AB, Eriksen EF, Ish-Shalom S, Genant HK, Wang O, Mitlak BH (2001) Effect of recombinant human parathyroid hormone (1–84) on vertebral fracture and bone mineral density in postmenopausal women with osteoporosis. N Engl J Med 344(19):1434–1441. https://doi.org/10.1056/NEJM200105103441904

Pastrama MI, Scheiner S, Pivonka P, Hellmich C (2018) A mathematical multiscale model of bone remodeling, accounting for pore space-specific mechanosensation. Bone 107(1):208–221. https://doi.org/10.1016/j.bone.2017.11.009

Peterson MC, Riggs MM (2010) A physiologically based mathematical model of integrated calcium homeostasis and bone remodeling. Bone 46(1):49–63. https://doi.org/10.1016/j.bone.2009.08.053

Pivonka P, Zimak J, Smith DW, Gardiner BS, Dunstan CR, Sims NA, Martin TJ, Mundy GR (2008) Model structure and control of bone remodeling: a theoretical study. Bone 43(2):249–263. https://doi.org/10.1016/j.bone.2008.03.025

Pivonka P, Zimak J, Smith DW, Gardiner BS, Dunstan CR, Sims NA, John Martin T, Mundy GR (2010) Theoretical investigation of the role of the RANK-RANKL-OPG system in bone remodeling. J Theor Biol 262(2):306–316. https://doi.org/10.1016/j.jtbi.2009.09.021

Pivonka P, Buenzli PR, Scheiner S, Hellmich C, Dunstan CR (2013) The influence of bone surface availability in bone remodelling: a mathematical model including coupled geometrical and biomechanical regulations of bone cells. Eng Struct 47:134–147. https://doi.org/10.1016/j.engstruct.2012.09.006

Riggs BL, Parfitt AM (2005) Drugs used to treat osteoporosis: the critical need for a uniform nomenclature based on their action on bone remodeling. J Bone Miner Res 20(2):177–184. https://doi.org/10.1359/JBMR.041114

Saag KG, Shane E, Boonen S, Marín F, Donley DW, Taylor KA, Dalsky GP, Marcus R (2007) Teriparatide or alendronate in glucocorticoid-induced osteoporosis. N Engl J Med 357(20):2028–2039. https://doi.org/10.1056/NEJMoa071408

Satterwhite J, Heathman M, Miller PD, Marín F, Glass EV, Dobnig H (2010) Pharmacokinetics of teriparatide (rhPTH[1-34]) and calcium pharmacodynamics in postmenopausal women with osteoporosis. Calcif Tissue Int 87(6):485–492. https://doi.org/10.1007/s00223-010-9424-6

Scheiner S, Pivonka P, Hellmich C (2013) Coupling systems biology with multiscale mechanics, for computer simulations of bone remodeling. Comput Methods Appl Mech Eng 254(1):181–196. https://doi.org/10.1016/j.cma.2012.10.015

Scheiner S, Pivonka P, Smith DW, Dunstan CR, Hellmich C (2014) Mathematical modeling of postmenopausal osteoporosis and its treatment by the anti-catabolic drug denosumab. Int J Numer Methods Biomed Eng 30(1):1–27. https://doi.org/10.1002/cnm.2584

Silva BC, Bilezikian JP (2015) Parathyroid hormone: anabolic and catabolic actions on the skeleton. Curr Opin Pharmacol 22(1):41–50. https://doi.org/10.1016/j.coph.2015.03.005

Subbiah V, Madsen VS, Raymond AK, Benjamin RS, Ludwig JA (2010) Of mice and men: divergent risks of teriparatide-induced osteosarcoma. Osteoporos Int 21(6):1041–1045. https://doi.org/10.1007/s00198-009-1004-0

Sugiyama T, Saxon LK, Zaman G, Moustafa A, Sunters A, Price JS, Lanyon LE (2008) Mechanical loading enhances the anabolic effects of intermittent parathyroid hormone (1-34) on trabecular and cortical bone in mice. Bone 43(2):238–248. https://doi.org/10.1016/j.bone.2008.04.012

Tanaka S, Sakai A, Tanaka M, Otomo H, Okimoto N, Sakata T, Nakamura T (2004) Skeletal unloading alleviates the anabolic action of intermittent PTH(1-34) in mouse tibia in association with inhibition of PTH-induced increase in c-fos mRNA in bone marrow cells. J Bone Miner Res 19(11):1813–1820. https://doi.org/10.1359/JBMR.040808

Trichilo S, Scheiner S, Forwood M, Cooper DM, Pivonka P (2019) Computational model of the dual action of PTH: application to a rat model of osteoporosis. J Theor Biol 473(1):67–79. https://doi.org/10.1016/j.jtbi.2019.04.020